Eur Biophys J
DOI 10.1007/s00249-012-0826-4

ORIGINAL PAPER

EBSA
Biophysics in Europe

Effect of cholesterol on the lateral nanoscale dynamics of fluid membranes

Clare L. Armstrong · Matthew A. Barrett · Arno Hiess · Tim Salditt · John Katsaras · An-Chang Shi · Maikel C. Rheinstädter

Received: 2 March 2012 / Revised: 3 May 2012 / Accepted: 7 May 2012

Abstract Inelastic neutron scattering was used to study the effect of 5 and 40 mol% cholesterol on the lateral nanoscale dynamics of phospholipid membranes. By measuring the excitation spectrum at several lateral $q_{\|}$ values (up to $q_{\|} = 3$ Å^{-1}), complete dispersion curves were determined of gel, fluid and liquid-ordered phase bilayers. The inclusion of cholesterol had a distinct effect on the collective dynamics of the bilayer's hydrocarbon chains; specifically, we observed a pronounced stiffening of the membranes on the nanometer length scale in both gel and fluid bilayers, even though they were experiencing a higher degree of molecular disorder. Also, for the first time we determined the nanoscale dynamics in the high-cholesterol liquid-ordered phase of bilayers containing cholesterol. Namely, this phase appears to be "softer" than fluid bilayers, but better ordered than bilayers in the gel phase.

Keywords Lipid membrane · Cholesterol · Lateral membrane dynamics · Nanoscale dynamics · Liquid-ordered phase · Inelastic neutron scattering · Dispersion relation

Special Issue: Scattering techniques in biology: marking the contributions to the field from Peter Laggner on the occasion of his 68th birthday.

C. L. Armstrong (✉) · M. A. Barrett · A.-C. Shi · M. C. Rheinstädter
Department of Physics and Astronomy, McMaster University, ABB-241, 1280 Main Street West, Hamilton, ON L8S 4M1, Canada
e-mail: armstc5@mcmaster.ca

A. Hiess
European Spallation Source ESS AB, P.O. Box 176, 22100 Lund, Sweden

T. Salditt
Institute for X-Ray Physics, Georg-August-University Göttingen, Friedrich-Hund-Platz 1, 37077 Göttingen, Germany

J. Katsaras
Neutron Sciences Directorate, Oak Ridge National Laboratory, Oak Ridge, TN 37831-6100, USA

J. Katsaras · M. C. Rheinstädter (✉)
Canadian Neutron Beam Centre, National Research Council, Chalk River, ON K0J 1J0, Canada
e-mail: rheinstadter@mcmaster.ca

Introduction

Cholesterol is an essential structural component of eukaryotic cell membranes capable of modulating their permeability and molecular organization. It is either obtained from foods of animal origin or synthesized in the endoplasmic reticulum, a multifold membranous structure that is also capable of producing phospholipids, including different types of membranes (Ridsdale et al. 2006). In association with lipid rafts (i.e., functional domains), cholesterol has also been implicated in cell signaling processes (Simons 1997; Brown 2000; Petrie et al. 2000; Papanikolaou et al. 2005; Pike 2006).

Cholesterol and saturated lipid species preferentially partition into liquid-ordered domains, away from unsaturated, liquid-disordered lipid species. In particular, cholesterol, because of its rigid planar structure, preferentially interacts with sphingolipids (e.g., sphingomyelin) and their highly ordered saturated hydrocarbon chains, but not exclusively (Pike 2009). Moreover, cholesterol has been shown to interact strongly with phosphatidylcholine (PC) lipids that have saturated hydrocarbon chains (Vist 1990).

Published online: 23 June 2012

In pure lipid bilayers, cholesterol modulates the molecular organization of lipids, namely by disrupting the regular packing of gel phase di-saturated PC membranes and restricting the reorientation of these same membranes when in the liquid-disordered phase (Vist 1990). However, at sufficiently high concentrations of cholesterol (i.e., >25 mol%), the so-called liquid-ordered state, which is characterized by rapid hydrocarbon chain reorientation but high conformational order, is formed over a wide range of temperatures smearing out the traditional gel and liquid crystalline phases (Fig. 1) (Mouritse 2010).

Although cholesterol is known to modulate the behavior of membranes, in the recent past it has been shown that lipid bilayers made of polyunsaturated fatty acids (PUFAs, namely, di-20:4 PC) can cause cholesterol to sequester to the bilayer center (i.e., laying flat with its hydroxyl group in the middle of the bilayer) (Harroun et al. 2006, 2008), a location that is significantly different from cholesterol's nominal upright orientation, where its hydroxyl group is located near the lipid/water interface (Léonard et al. 2001). However, the addition of just 5 mol% of dimyristoyl phosphatidylcholine (DMPC, di-14:0 PC) to those same PUFA bilayers causes cholesterol to revert to its nominal upright orientation (Kučerka 2009). This has been explained in terms of the "umbrella" model (Petrie et al. 2000; Papanikolaou et al. 2005), which suggests that cholesterol molecules associate strongly with ordered hydrocarbon chains (usually ones that are fully saturated) in such a manner that they are shielded from contact with the aqueous environment by the lipid head group. It seems obvious then that, although cholesterol can modulate the structural (e.g., chain packing) and mechanical (e.g., bending modulus) properties of bilayers, the bilayers themselves can, on the other hand, also modulate cholesterol's behavior.

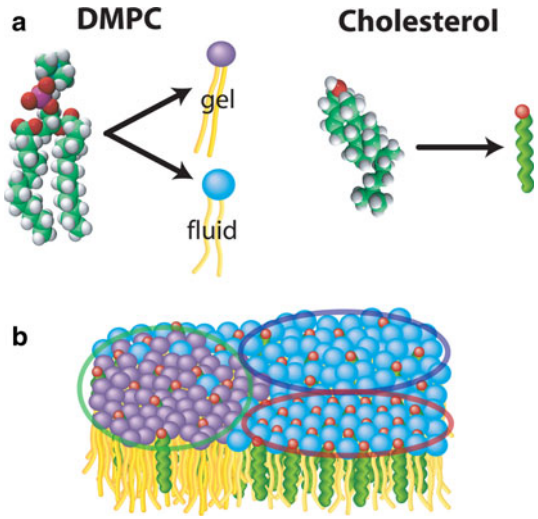

Fig. 1 **a** Schematic representations of DMPC and cholesterol molecules. In the gel phase, the lipids tails are in the all-trans configuration. At the main transition temperature lipid hydrocarbon tails "melt", resulting in fluid phase bilayers. **b** Schematic model of the possible phases present in DMPC/cholesterol systems. The gel, fluid and liquid-ordered phases are highlighted by the *green*, *blue* and *red circles*, respectively

We have studied the short wavelength fluctuations in DMPC membranes containing 5 and 40 mol% cholesterol using inelastic neutron scattering. Complete dispersion relations of gel, fluid and liquid-ordered membranes were obtained by measuring the excitation at different lateral momentum transfers. From experimentally obtained spectra, we were able to extract the "softness" of the hydrocarbon membrane core on the nanometer length scale, a length scale comparable to molecular distances within the membrane. We found that the bilayer's hydrocarbon core became significantly less fluid in the presence of cholesterol. In the liquid-ordered state, however, the system not only assumed a high degree of molecular order (associated with the high cholesterol content), but there was a concomitant softening of the nanoscale elastic properties, a feature more akin to fluid bilayers.

Materials and methods

Sample preparation

Highly oriented multi-lamellar stacks of 1,2-dimyristoyl-sn-glycero-3-phosphocholine (DMPC) and cholesterol were prepared on 2-inch-diameter, 300-μm-thick, single-side polished Si wafers. The coherent scattering of the lipid hydrocarbon chains was enhanced by using tail deuterated lipids, i.e., DMPC-d54. The use of protonated cholesterol enabled the experiment to detect changes in hydrocarbon chain structure and dynamics. A 20 mg/ml suspension of DMPC-d54 and cholesterol dissolved in 1:1 chloroform and 2,2,2-trifluoroethanol (TFE) was prepared. Two different samples were fabricated for this study; specifically, a sample containing 5 mol% cholesterol and another with 40 mol% cholesterol, a concentration found in biological membranes. The Si wafers were cleaned by alternate 12-min sonications in ultra-pure water and ethanol at 313 K. This process was repeated twice. Then 1 ml of the lipid solution was deposited on each Si wafer and allowed to dry. The wafers were kept in a vacuum overnight to remove all traces of the solvent. The samples were then hydrated with heavy water (D_2O) and annealed at 303 K for 24 h. Following this protocol, each wafer contained roughly 3,000 highly oriented membranes, totaling $\sim$10 μm in thickness.

Twenty sample-containing Si wafers were stacked with 0.6-mm aluminium spacers placed in between each wafer to enable proper hydration of the membranes. The stack of

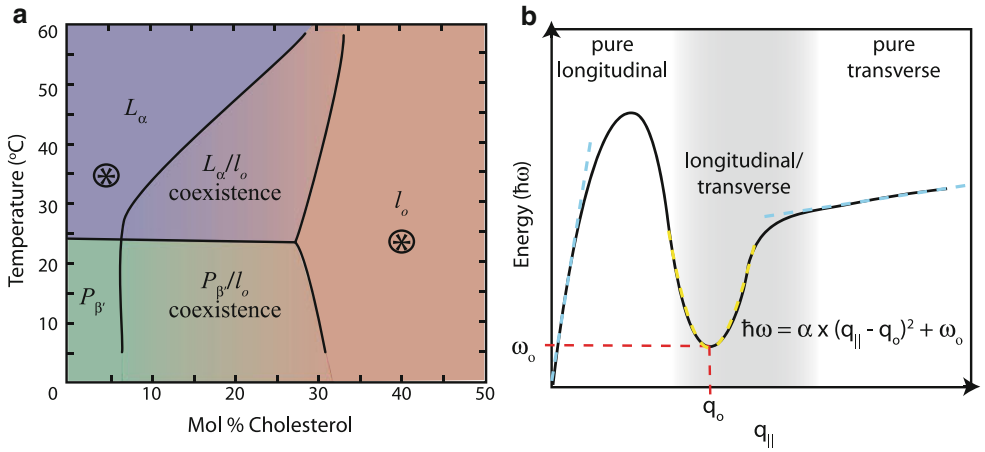

Fig. 2 **a** Schematic phase diagram of a DMPC cholesterol system as reported by, e.g., Vist 1990; Almeida et al. 1992; Thewalt and Bloom 1992; de Meyer 2009; de Meyer et al. 2010. Besides the well-known gel and fluid phase, the so-called liquid-order phase, is observed at high cholesterol concentrations. The 5 mol% cholesterol sample is in the L_α phase, while the 40 mol% sample is clearly in the l_o phase, as depicted by the ⊛. **b** A typical lateral dispersion curve observed in lipid systems (see, e.g., Chen et al. 2001; Weiss et al. 2003; Chen et al. 2003; Rheinstädter et al. 2004a; Tarek et al. 2001; Hub et al. 2007; Kaye et al. 2011). The $q_{||}$ range around the minimum is well described by a parabolic fit. The dispersion is linear at small $q_{||}$ values due to high-frequency sound propagation with longitudinal polarization. The high-$q_{||}$ regime is also linear; however, a transverse polarization has been previously observed

Si wafers were kept in a temperature- and humidity-controlled aluminium chamber, a so-called humidity chamber, during the course of the experiment. Hydration of the lipid membranes from the vapor phase was achieved by separately adjusting the temperature of the heavy water reservoir, the "sandwich" stack of Si wafers and the sample chamber's cover. Temperature and humidity sensors were installed close to the sample, and a water bath was used to control the temperature of the water reservoirs. Using this setup, a lamellar repeat spacing (d_z-spacing) of 53.1 Å was achieved for the fluid phase low cholesterol sample, which is comparable to the fluid phase of pure DMPC. For example, from the published values for d_z as a function of relative humidity (RH) published for pure DMPC (Kučerka 2005), the hydration of the DMPC bilayers in this experiment is estimated to be ∼99.5% (100% RH corresponds to fully hydrated bilayers) (Katsaras 1998).

The samples were mounted vertically in the neutron beam such that the scattering vector (**Q**) could either be placed in the plane of the membrane ($\mathbf{q}_{||}$) or perpendicular to the membrane ($\mathbf{q}_z$). Out-of-plane and in-plane structure could be measured by simply rotating the sample by 90°.

The phase diagram of phospholipid membranes containing different amounts of cholesterol remains an active field of research (Vist 1990, Almeida et al. 1992; Thewalt and Bloom 1992; de Meyer 2009; de Meyer et al. 2010). A schematic phase diagram of DMPC/cholesterol membranes is shown in Fig. 2a. It has been speculated that the relatively stiff cholesterol molecules align parallel to the hydrocarbon lipid tails and suppress lipid tail fluctuations (Róg et al. 2009), thereby affecting the membrane's dynamical properties. Most studies agree that three phases are observed, depending on temperature and cholesterol concentration: the rigid gel (ripple) $P_{\beta'}$ phase, the fluid L_α phase and the liquid-ordered l_o phase. The gel and fluid phases are well known from single component phospholipid bilayers. However, the l_o phase is solely observed at high concentrations of cholesterol. This bilayer phase is somewhat peculiar as it appears to be well ordered (similar to the gel phase); however, the lipids exhibit a diffusion coefficient that is comparable to that of fluid bilayers.

At low cholesterol content the bilayers undergo a phase transition from the gel to the fluid phase, as in pure lipid bilayers. The temperature of this so-called main transition T_m is slightly shifted towards higher temperatures. However, at high cholesterol concentrations ($\gtrsim$40 mol%), the main transition of liquid-ordered membranes was found to be suppressed, while at intermediate cholesterol concentrations (i.e., between about 10–30 mol%) most studies report a coexistence between gel and l_o, or L_α and l_o phases. The 5 mol% cholesterol sample was measured at $T = 308$ K (35 °C), while all scans for the 40 mol% sample were conducted at $T = 297$ K (24 °C). These temperatures were selected based on the schematic phase diagram in Fig. 2a. In an attempt to measure the system in one phase, temperatures were chosen far from the speculated phase boundaries. The phases at which these samples were studied are shown in Fig. 2a. The 5 mol% sample is, therefore, made up of fluid phase DMPC bilayers. As the phase transition was found to be suppressed in the l_o phase, the temperature is not a critical parameter for the high cholesterol sample.

Neutron-scattering experiment

Experiments were conducted using two different triple-axis spectrometers (TAS) co-located at the Institut Laue-Langevin high flux neutron reactor (Grenoble, France). The three axis of the spectrometers refer to the axes of rotation of the monochromator, the sample and the analyzer. The incident and final neutron energies are defined by the Bragg reflections from pyrolytic graphite (PG) crystals. Divergence of the neutron beam is controlled by several neutron Soller collimators. A schematic of the instrument configuration is shown in Fig. 3. In-plane and out-of-plane structure and dynamics can be measured simultaneously on a TAS by simply rotating the sample by 90°.

Neutrons with energies up to 20 meV were measured on the thermal TAS IN8 instrument with an energy resolution of $\sim$1 meV. Cold neutron spectrometers are inherently higher energy resolution instruments and enable the measurement of low-energy excitations (up to $\sim$5 meV). These measurements were conducted on the cold TAS IN12, which has an energy resolution of $\sim$0.2 meV.

The energy and $q_{||}$ resolution of a neutron triple-axis spectrometer are determined by the incident neutron energy, the divergence of the neutron beam and the wavelength resolution of the monochromator and analyzer. The incident energies, energy range, $q_{||}$ range and resolution of the two spectrometers used for this study are listed in Table 1. By combining a cold and thermal TAS, a $(\hbar\omega, q_{||})$ range of 0.4 Å^{-1} $< q_{||} <$ 3 Å^{-1} and energies of up to $\sim$20 meV were accessible. As a result, our experiments were sensitive to picosecond dynamics in the plane of the membrane, covering length scales from between 2 and $\sim$20 Å. These distances range from less than a lipid-lipid interaction to one encompassing almost three lipid molecules.

Results

Neutron diffraction

Our setup permitted for the determination of the out-of-plane and in-plane structure of 2 mol% cholesterol/membrane samples. By rotating the sandwich sample by 90°, the scattering geometry can be switched (with respect to the Si substrates) from transmission to grazing incidence. To study in-plane structure ($\mathbf{q}_{||}$), the scattering vector $\mathbf{Q}$ is located in the plane of the membrane (i.e., transmission geometry). In grazing incidence, $\mathbf{Q}$ is normal to the Si and membrane plane ($\mathbf{q}_z$), enabling us to study out-of-plane structure.

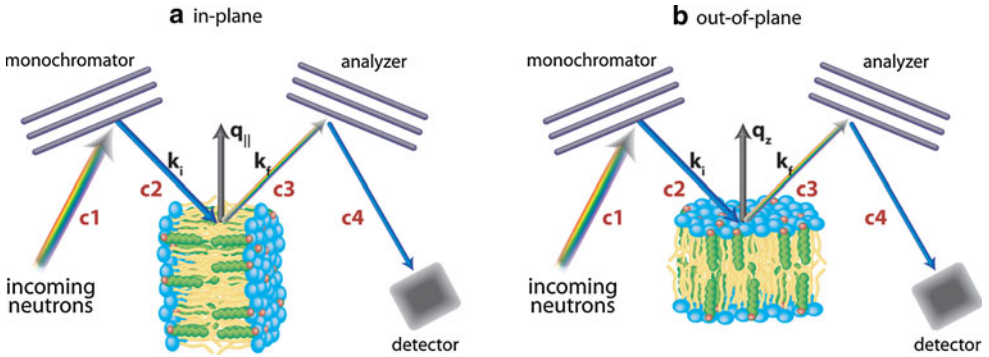

Fig. 3 Schematic representation of a triple axis spectrometer geometry. **a** Orientation of the sample for in-plane scans such that $\mathbf{Q}$ is in the plane of the membrane ($\mathbf{q}_{||}$). **b** Orientation of the sample for out-of-plane scans such that $\mathbf{Q}$ is perpendicular to the plane of the membrane ($\mathbf{q}_z$). $\mathbf{k_i}$ and $\mathbf{k_f}$ are the incident and final wave vectors, respectively; $c1$–$c4$ indicate the positions of the neutron collimators that were used to control the $\mathbf{Q}$ and energy resolutions

Table 1 $q_{||}$ and q_z and energy resolutions of the two spectrometers used in this study

Instrument	Incident neutron energy (meV)	Accessible energy range (meV)	Energy resolution (meV)	Accessible $q_{||}$ range (Å^{-1})	$q_{||}$ resolution (Å^{-1})
IN12	4.7	0–5	0.165	0–3	0.01
IN8	14.7	0–25	1.01	0–3	0.02

Instrumental setup, including collimation, was 30′–monochromator–30′–sample–30′–analyzer–60′–detector on IN12 and ø–monochromator–30′–PG filter–sample–30′–analyzer–ø–detector on IN8

In-plane structure

The lipid acyl chain positional correlation peak is the result of closely packed acyl chains making up the hydrophobic core of the membrane, as shown in Fig. 4a. The Bragg peaks from the two samples are well fit by Lorentzians. The peak in the 40 mol% sample is more pronounced and slightly shifted toward smaller $q_{||}$-values. This implies an enhanced order of the lipid tails at 40 mol% cholesterol. The distance between two lipid chains increases from 4.53 Å ($q_{||} = 1.39$ Å^{-1}) to 4.59 Å ($q_{||} = 1.37$ Å^{-1}), as determined from the fits to the Bragg peaks ($d = 2\pi/q_{||}$). The widths of the Bragg peaks also increase, albeit slightly, from $\Delta q_{||} = 0.13$ Å^{-1} to $\Delta q_{||} = 0.14$ Å^{-1}, which indicates a larger distribution of nearest-neighbor distances. The presence of cholesterol molecules seems to have little effect on hydrocarbon chain packing. The packing of lipid acyl chains is the result of a balance between attractive and repulsive forces resulting from tail fluctuations, i.e., between the free energy and entropy of the hydrocarbon tails. Incorporation of cholesterol molecules should, in theory, drastically increase the area per lipid. However, the area per lipid in the presence of cholesterol is comparable to lipid areas found in pure lipid bilayers, as cholesterol is believed to suppress hydrocarbon chain fluctuations.

It should be noted that the curves in Fig. 4a have not been shifted with respect to each other. The background in the 40 mol% sample is drastically increased because of the presence of protonated cholesterol, which contributes to the strong incoherent background.

Out-of-plane structure

Specular reflectivity allows for the determination of bilayer structure perpendicular to the plane of the membrane [see, e.g., Pabst 2010; Fragneto 2007]. The intensity of the

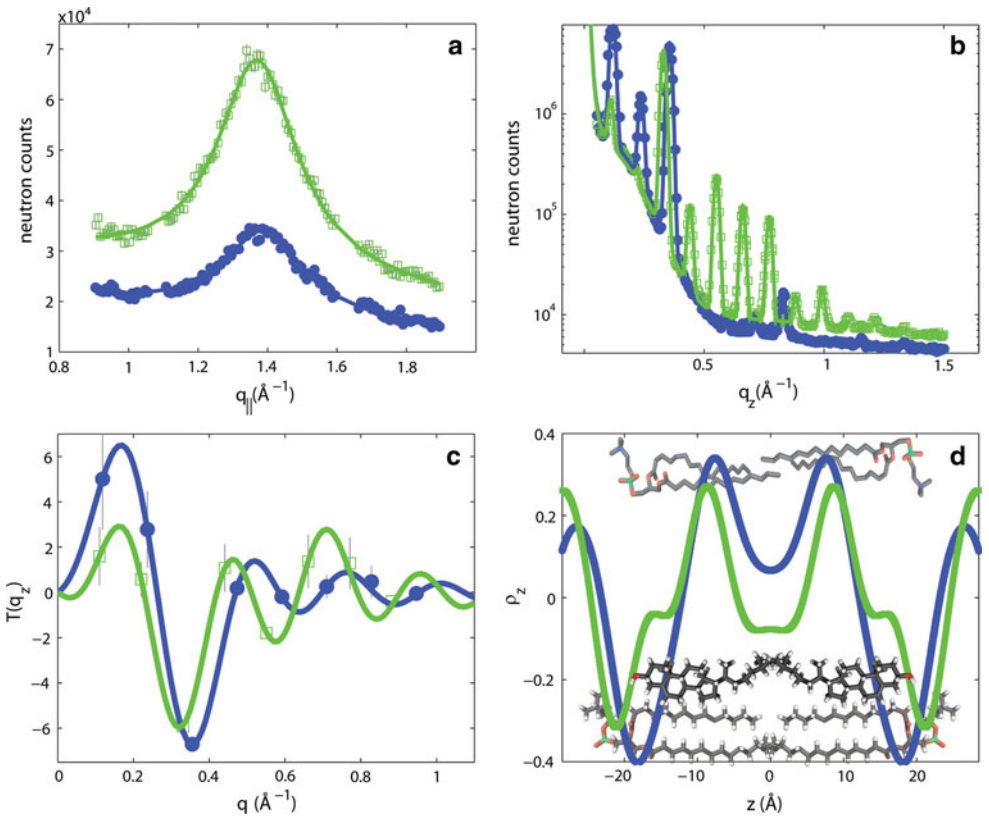

Fig. 4 Overview of the diffraction data: the *blue solid lines* and data points correspond to the 5 mol% cholesterol sample, while the *green solid lines* and data points refer to the 40 mol% cholesterol sample. **a** In-plane scattering ($q_{||}$) used to measure the acyl chain-chain positional correlation peak. Two spurious Bragg peaks from the humidity chamber at ~1.1 Å^{-1} and ~1.65 Å^{-1} were omitted from the scans. The *solid lines* are the Lorentzian fits to the experimental data. **b** Out-of-plane scattering (q_z) and the observation of several Bragg peaks. The position and area of each Bragg peak was determined through the fitting of a Gaussian, including the q^{-4} background. **c** $T(q_z)$, as determined by Eq. (4). Data points correspond to the integrated intensities of the different out-of-plane Bragg peaks from (**b**). The phases ν_n are determined by the sign of $T(q_z)$ at the q_z position of the corresponding Bragg reflection. **d** Scattering density profile, ρ_z, calculated using Eq. (3). The location of the cholesterol molecules within the lipid bilayer can be deduced by the ρ_z of the two different mol% cholesterol membranes (5 mol%, blue; 40 mol%, *green*). Lipid and cholesterol molecules are shown schematically. The data shown were collected using the IN8 thermal TAS

reflected beam as a function of the perpendicular momentum transfer, q_z, is given by:

$$R(q_z) = \frac{16\pi^2}{q_z^2}|\hat{\rho}(q_z)|^2, \quad (1)$$

where $\hat{\rho}(q_z)$ is the one-dimensional Fourier transform of the neutron scattering length density and is defined by:

$$\hat{\rho}(q_z) = \int_{-\infty}^{\infty} \exp(iq_z z)\rho(z)dz. \quad (2)$$

Because the membranes are stacked (i.e., there is a convolution with the lamellar structure factor), the Fourier transform is not continuous, but discrete. The different Fourier components are observed in the experiment as the integrated intensities of the out-of-plane Bragg peaks. $\rho(z)$ is approximated by a 1D Fourier analysis (Tristram-Nagle et al. 2002) as follows:

$$\begin{aligned}\rho(z) &= \rho_W + \frac{F(0)}{d_z} + \frac{2}{d_z}\sum_{n=1}^{N} F(q_n)v_n \cos(q_n z) \\ &= \rho_W + \frac{F(0)}{d_z} + \frac{2}{d_z}\sum_{n=1}^{N} \sqrt{I_n q_n}\, v_n \cos\left(\frac{2\pi n z}{d_z}\right), \end{aligned} \quad (3)$$

where N is the highest order Bragg peak observed experimentally, and ρ_W is the scattering length density of bulk water. The integrated peak intensities, I_n, are multiplied by q_n to retrieve the form factors, $F(q_n)$ (Nagle 1989, Nagle et al. 1996). We note that Eq. (3) is used to calculate absolute scattering length densities if the curves are normalized by using $F(0)$ and ρ_W. As the setup used in this study is not optimized for quantitative reflectivity measurements, we present relative rather than absolute scattering length densities. By comparing the two samples, these measurements can be used to determine the position of molecules within the bilayers, as will be shown below.

The bilayer form factor $F(q_z)$, which is in general a complex quantity, is real in the case of centro-symmetry. The ubiquitous crystallographic phase problem, therefore, simplifies to $F(q_z) = \pm|F(q_z)|$, where the phases, v_n, can only take on values of ± 1. Assigned values for v_n are needed to reconstruct the scattering length density profile from the data following Eq. (3). When the membrane form factor $F(q_z)$ is measured at several q_z values, a continuous function, $T(q_z)$, which is proportional to $F(q_z)$, can be fit to the data (Nagle 1989; Nagle et al. 1996; King 1971; Adachi 2000):

$$T(q_z) = \sum_n \sqrt{I_n q_n}\ \mathrm{sinc}(\pi d_z q_z - \pi n). \quad (4)$$

Once an analytical expression for $T(q_z)$ has been determined from fitting the various Bragg peaks, the v_n values can be determined from $T(q_z)$. The d_z-spacing between two neighboring membranes in the stack can be determined from the positions of the Bragg reflections ($d_z = 2\pi/\Delta q_z$) along the out-of-plane axis, q_z.

Figure 4b shows out-of-plane scans for the 5 and 40 mol% cholesterol samples. Up to ten distinct Bragg peaks are observed and are used to reconstruct the scattering length density. Figure 4c, d displays $T(q_z)$ and relative scattering length densities as determined using Eqs. (4) and (3). $T(q_z)$ was fitted to the experimentally determined peak intensities using Eq. (4) to calculate an array of v_n values out of the corresponding 2^{10} combinations, assuming a phase of $+1$ or -1. Figure 4c shows the best fits to the data. Both samples were well fitted using the following combination of phases: $11\bar{1}1\bar{1}1\bar{1}1\bar{1}$. The resulting scattering length densities are plotted in Fig. 4d. This type of sample preparation (chain deuterated lipids hydrated by heavy water) accentuates the water contribution, i.e., the layer between the membranes at $\sim$24 Å. The minima at about 20 Å correspond to the protonated lipid head groups. The scattering length density then increases toward the bilayer centre, i.e., $z = 0$. The sharp dip at the centre of the 5 mol% cholesterol sample is the tell-tale sign of a fluid membrane, i.e., the increasing number of kink-defects lower the density of the lipid tails in the bilayer centre.

At 40 mol% cholesterol, a peak at $\sim$18 Å appears, and the density at the membrane centre experiences a further decrease, showing a plateau, however, instead of a dip. Lipid and cholesterol molecules can tentatively be fit to this structure, and are schematically illustrated in Fig. 4d. The peak at $\sim$18 Å is most likely related to the presence of the hydrophilic head of the cholesterol molecule (Léonard et al. 2001). Since cholesterol makes up 40 mol% of the membrane, the density of carbon atoms in the centre of the membrane is further reduced, as cholesterol has a single chain compared to the two acyl chains of a lipid molecule. It seems, however, that the presence of cholesterol suppresses lipid tail fluctuations, as the scattering length density in the membrane centre remains constant. Our data (Fig. 4) support the notion that cholesterol molecules assume an upright orientation (Léonard et al. 2001) with their hydrophilic head residing in the lipid head group region. The data in Fig. 4 are in excellent agreement with neutron diffraction results in cholesterol-containing polyunsaturated lipid membranes (18:0-22:6n3-PC) (Mihailescu et al. 2011), where the cholesterol molecule was also found in an upright position. This observation is also consistent with the commonly accepted umbrella model of cholesterol interaction with lipid bilayers (Huang 1999).

Membrane dynamics

Motions in lipid membranes range from long wavelength undulation and bending modes, with typical relaxation

times on the order of nanoseconds and lateral length scales of several hundred lipid molecules (i.e., tens of nanometers), to short wavelength density fluctuations in the picosecond range and nearest-neighbor length scales (Rheinstädter et al. 2004a, Pfeiffer et al. 1989; König et al. 1992; Pfeiffer et al. 1993; König et al. 1994, 1995; Lipowsky and Sackmann 1995; Lindahl and Edholm 2000; Bayerl 2000; Salditt 2000; Rheinstädter et al. 2005, 2006, 2007) Different techniques have been used to study the different types of motions. For example, local dynamics in lipid bilayers (i.e., individual lipid molecules), such as vibration, rotation, libration (hindered rotation) and diffusion, have been investigated by incoherent neutron scattering (König et al. 1992, 1994, 1995; Pfeiffer et al. 1993; Meinhold et al. 2007) and nuclear magnetic resonance (NMR) (Bloom and Bayerl 1995; Nevzorov and Brown 1997) in order to determine the short wavelength translational and rotational diffusion constants. On the other hand, collective bilayer undulations have been examined by coherent scattering experiments using neutron spin-echo spectrometers (Pfeiffer et al. 1993, Rheinstädter et al. 2005, Meinhold et al. 2007, Takeda et al. 1999) and Dynamic Light Scattering (DLS) (Hirn et al. 1999; Hirn and Bayerl 1999; Hildenbrand and Bayerl 2005). TAS has been shown to be a well suited technique for the study of collective membrane dynamics (Rheinstädter et al. 2004a; Kaye et al. 2011; Rheinstädter et al. 2006b; Rheinstädter et al. 2009; Armstrong et al. 2011; Rheinstädter et al. 2004; Rheinstädter 2008). The dynamics that we are interested in are the propagation of short-wavelength density waves in the plane of the membrane, which can be thought of in terms of phonon-like excitations. These collective molecular motions determine, for instance, the elasticity of membranes (Rheinstädter et al. 2006a) and are speculated to be relevant for interactions between membrane embedded proteins (Rheinstädter et al. 2009) and membrane transport properties (Rheinstädter et al. 2004a; Kaye et al. 2011; Paula et al. 1996). Propagating modes lead to peaks in the neutron spectra at well-defined excitation energies. By measuring the excitation energies at different $q_{\|}$ values, i.e, different length scales, complete dispersion relations can be determined. However, we would like to point out that these types of dynamics are different from relaxational dynamics. A well-known example of a relaxation process in lipid membranes is the diffusion of lipids and other molecules in the plane of the membrane. The eigenfrequency of a relaxation dynamic is $\hbar\omega = 0$, which leads to a quasi-elastic broadening of the central line of the neutron spectra. Relaxational dynamics are usually slow (on the order of nano- to microseconds), while the propagating modes take place on the picosecond time scale. The two types of dynamics can be well distinguished in inelastic neutron scattering experiments. For example, diffusion is determined by measuring the broadening of the quasi-elastic peak, while in the case of propagating wave-like excitations (which are of particular interest to us), they are observed as inelastic peaks at excitation energies $\hbar\omega \neq 0$ meV.

A typical lipid dispersion relation in lipid membranes is shown in Fig. 2b. This in-plane dispersion relation was determined using several techniques in DMPC and DLPC—i.e., inelastic X-ray scattering (Chen et al. 2001, 2003; Weiss et al. 2003), inelastic neutron scattering (Rheinstädter et al. 2004a, Rheinstädter et al. 2004) and molecular dynamics (MD) simulations (Tarek et al. 2001; Hub et al. 2007; Kaye et al. 2011). The lipid dispersion curve has a generic shape, namely at small $q_{\|}$ values (long length scales) there is a linear region $\hbar\omega \propto q_{||}$ as the excitation propagates in the form of long-wavelength sound waves. The dispersion then goes through a maximum before a minimum is observed close to the nearest-neighbor distance (~ 1.5 Å^{-1}) of two lipid acyl tails. Beyond this minimum, a second linear regime is observed at high $q_{\|}$. Recently Kaye et al. 2011. studied the polarization of these excitations by combining neutron scattering and MD simulations. In a longitudinal wave, the C-atoms of the hydrocarbon tails are displaced along the direction of the propagating wave—in a transverse wave, particles are displaced perpendicular to the propagation direction. According to Kaye et al. (2011), the long-wavelength modes are purely longitudinal in nature. At high in-plane momentum transfers $q_{\|}$ (i.e., beyond the dispersion minimum), pronounced transverse properties were observed. However, in the vicinity of the dispersion minimum, the excitations have a mixed, longitudinal and transverse character. Because these excitations have been associated with the transport of small molecules in bilayers (Paula et al. 1996), the longitudinal and transverse fluctuations have been speculated to be relevant for the in-plane and trans-membrane transport of small molecules, such as water (Kaye et al. 2011, Paula et al. 1996).

Two types of inelastic scans were conducted. Specifically, constant-$q_{\|}$ scans, in which a $q_{\|}$ value is selected and held constant while the energy transfer $\hbar\omega$ is scanned, and constant-energy scans, for which the spectrometer is tuned to a certain energy transfer, $\hbar\omega$, and the momentum transfer $q_{\|}$ is varied. Both types are usually employed to measure dispersion relations. As a general rule, energy scans are usually used when the dispersion relation is flat. On the other hand, constant-$q_{\|}$ scans are usually better suited to measure steep parts of the dispersion. Examples of constant-energy and constant-$q_{\|}$ scans are shown in Fig. 5. The position of the excitations as function of $\hbar\omega$ and $q_{\|}$ is then determined from the positions of peaks in these scans. The constant-energy scans at $q_{\|} = 1.2$ Å^{-1} in Fig. 5a show two well-defined peaks at ~ 1.3 and ~ 2.1 meV in the

5 mol% cholesterol sample. Four peaks can be fit to the spectrum at a higher cholesterol concentration (as shown in Fig. 5b) at energies between 1 and 4 meV. The corresponding fitting functions consist of narrow Gaussian components centered at an energy transfer $\hbar\omega = 0$, which are used to describe the instrumental energy resolution (see Table 1), a broader Lorentzian component as a result of relaxational dynamics (also present in the systems studied) and damped harmonic oscillators (dho) for the excitations.

Figure 5c depicts constant-$q_{\|}$ scans in the two samples. Both scans show a broad component centered at $\sim q_{\|} = 1.38$ Å^{-1} and two narrow satellite peaks. As will be shown below, the broad peak is related to a minimum in the dispersion relation, i.e, a flat, horizontal region, while the narrow peaks are associated with the steeper branches. The solid lines in Fig. 5c are fits using Gaussian peak profiles—two narrow and a broad Gaussian peak were fitted to the two scans.

The use of a thermal TAS increases the available energy range. Figure 5d shows energy scans at $q_{\|} = 3$ Å^{-1} and an energy transfer of up to 20 meV. An excitation at $\sim$16 meV is visible as a pronounced peak in the spectra. This excitation was predicted by Tarek et al. (2001) and refers to an optical phonon associated with the dynamics of the terminal methyl end groups. The observed energy values are in excellent agreement with the theoretical values.

Several constant-$q_{\|}$ and constant-energy scans were performed on the two spectrometers to carefully scan the accessible energy and $q_{\|}$ range for excitations. These excitations could be assigned to dynamics in the gel, fluid and liquid-ordered states of the membrane.

Dispersion relations

Figure 6 shows all of the measured excitations (as function of energy transfer $\hbar\omega$ and momentum transfer $q_{\|}$) in the 5 and 40 mol% cholesterol samples as determined from the inelastic scans shown in Fig. 5. Excitation data measured using the cold and thermal TAS are depicted by circular

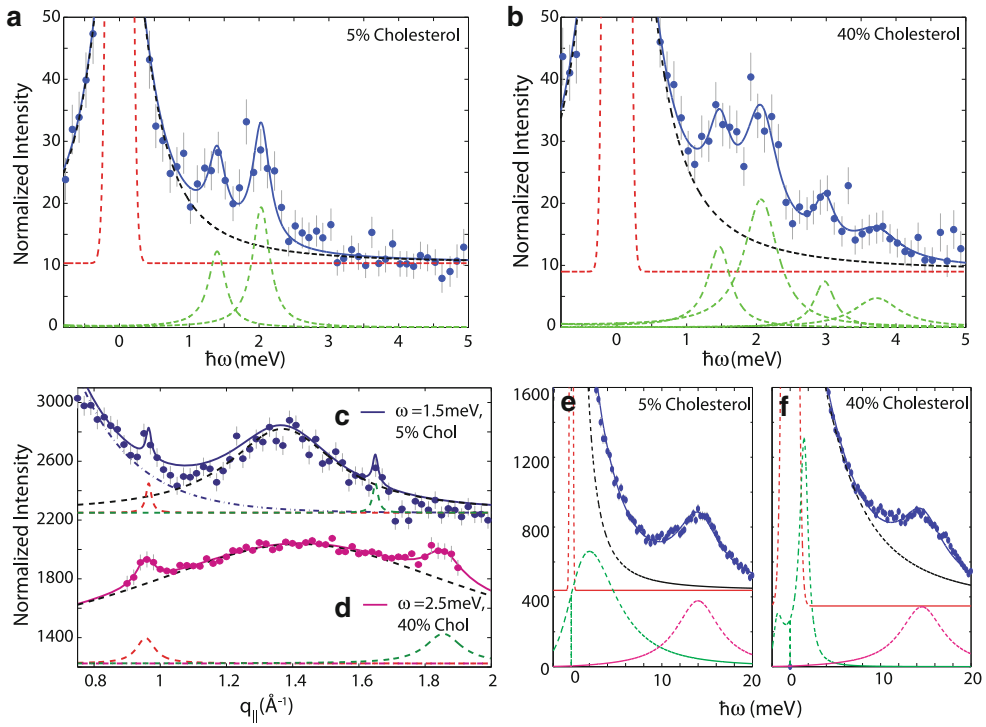

Fig. 5 Overview of the inelastic data: constant-$q_{\|}$ scan at $q_{\|} = 1.2$ Å^{-1}. The instrumental resolution is fit with a Gaussian (*red*), and the relaxation dynamics by a Lorentzian (*black*) function. The satellite excitations peaks are fit with damped harmonic oscillators (*green*), with the total fit shown in *blue*. **a** Data of 5 mol% and **b** 40 mol% cholesterol concentration samples. Constant-energy scan showing peaks fitted with Lorentzian curves: **c** 5 mol% cholesterol at $\hbar\omega$ = 1.5 meV. The Lorentzian fits are depicted by *dashed black*, *red* and *green curves*, with an exponential used to fit the background (*dashed blue*). The total fit is shown as a *solid blue line*. **d** 40 mol% cholesterol at $\hbar\omega$ = 2.5 meV. The Lorentzian fits are indicated by *dashed black*, *red* and *green curves*, with the constant background and the total fit depicted by *dashed magenta* and *solid magenta lines*, respectively. High-energy constant-$q_{\|}$ scans at $q_{\|} = 3$ Å^{-1}—the instrumental resolution is fit using a Gaussian (*red*), while a Lorentzian (*black*) function is used to describe the relaxation dynamics. The satellite excitation peaks are fit with damped harmonic oscillators (*green and magenta*), with the total fit shown in *blue*. **e** 5 mol% and **f** 40 mol% cholesterol concentrations. The green curves correspond to the low energy excitations from *a*, *b* and *c*, which cannot be resolved using the high-energy setup

and diamond-shaped symbols, respectively. The excitations were grouped into three different dispersion relations as follows: Pronounced and narrow excitations were assigned to the gel phase as the more ordered state of the lipid tails is expected to lead to well-defined excitations. Broad inelastic peaks are more likely the result of fluctuations in the fluid phase. The corresponding dispersion relations are similar to those shown in Fig. 2b. There was, however, a set of excitations (Fig. 6) that did not follow the gel or fluid dispersion curves, and was clearly outside of the error bars for those excitations. We tentatively assigned those excitations to the liquid-ordered state.

The data for the 5 mol% cholesterol sample (Fig. 4a) can be compared to the dispersion relations for gel and fluid DMPC and DPPC bilayers, as previously reported from inelastic X-rays (Chen et al. 2001, 2003; Weiss et al. 2003), neutron scattering (Rheinstädter et al. 2004a; Kaye et al. 2011) and MD simulations (Tarek et al. 2001; Hub et al. 2007). The shape of the gel dispersion curve agrees very well with ones in the literature. The energy value in the dispersion minimum is slightly increased (from 1 meV to $\sim$1.5 meV) in the presence of cholesterol. Only one excitation could clearly be identified at $q_{||}$ values of $\lesssim 0.9\,\text{Å}^{-1}$, and we assigned this excitation to the gel phase as we expect it to be the most pronounced. Therefore, the fluid and liquid-ordered dispersion relations do not have data points below $q_{||} \sim 1\,\text{Å}^{-1}$. As reported previously (Rheinstädter et al. 2004a), compared to the gel dispersion curve, the fluid dispersion curve appears to be less pronounced, with a higher energy value in the dispersion minimum, and lower (softer) energies at high $q_{||}$ values. This new dispersion curve, which we assigned to the liquid-ordered state shows, not only a very low minimum energy, but also very low energy values at high $q_{||}$.

All energy values for the 40 mol% cholesterol sample appear to be shifted to higher energies (Fig. 6b), the trademark of more rigid interactions, which lead to higher eigenfrequencies. In both the high and low cholesterol samples, three dispersion curves could be identified and assigned to the gel, fluid and tentatively to the liquid-ordered phases. In order to analyze the differences between the different states in the low and high cholesterol samples, the energy values around the dispersion minimum were fitted using a parabola:

$$\hbar\omega = \alpha \times (q_{||} - q_0)^2 + \omega_0. \tag{5}$$

The region around the minimum of the dispersions shown in Fig. 6 was fitted using Eq. (5). The fitted values for α and ω_o are listed in Table 2.

Because the bilayers were hydrated by heavy water, the experiment is potentially also sensitive to collective hydration water dynamics. We note, however, that we expect the corresponding signals to be small. The range of hydration water excitations, as reported from inelastic neutron scattering (Paciaroni et al. 2008), is shown in Fig. 6a, b. Two of the data points in Fig. 6b can most likely be assigned to hydration water dynamics.

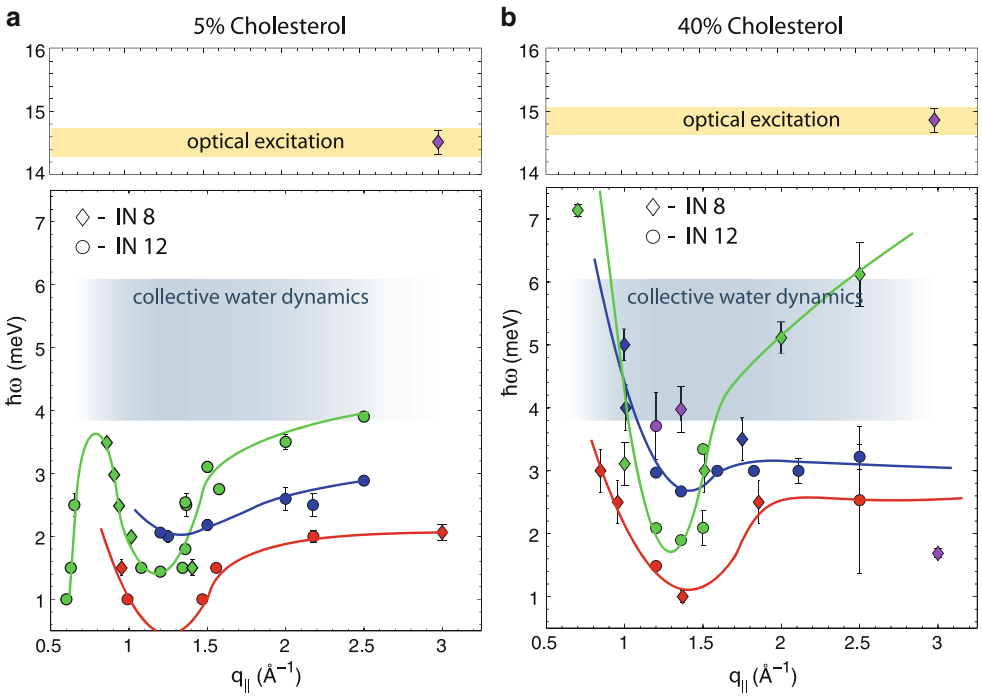

Fig. 6 Energy dispersion curves for DMPC bilayers with **a** 5 mol% cholesterol and **b** 40 mol% cholesterol. The dispersion curve corresponding to the gel phase is shown in *green* and the fluid phase in *blue*. The liquid-ordered phase, arising from the high concentration of cholesterol in the sample, is depicted by the *red curve*. The *blue band* at $\sim$4–6 meV represents the region where excitations due to hydrating water are observed (Paciaroni et al. 2008). The *yellow band* represents an optical excitation at 14–15 meV, which was predicted by MD simulations (Tarek et al. 2001)

Table 2 Results of parabolic fits using Eq. (5) to the dispersion minima in Fig. 6

	α (meV × Å^2)		ω_0 (meV)	
	5 mol% chol	40 mol% chol	5 mol% chol	40 mol% chol
Gel	16.3	30.3	1.38	1.80
Fluid	4.9	10.7	1.99	2.63
Liquid-ordered l_o	9.8	6.6	0.44	1.09

α is the slope of the parabola, and ω_0 is the energy offset. α can be thought of as a nanoscale bilayer "stiffness" on length scales corresponding to lipid tail-tail distances

Discussion

The lateral short-wavelength dynamics of the lipid tails in the hydrophobic membrane core have previously been studied in DMPC (Weiss et al. 2003; Chen et al. 2003; Rheinstädter et al. 2004a; Hub et al. 2007; Brüning et al. 2010; Kaye et al. 2011) and DLPC (Chen et al. 2001; Tarek et al. 2001) membranes, and the corresponding dispersion relations have been determined by inelastic X-ray scattering (IXS), inelastic neutron scattering and computer simulations. In this article we have determined complete energy dispersion curves for a DMPC membrane containing different amounts of cholesterol, a system previously studied by IXS (Weiss et al. 2003; Chen et al. 2003). The shape of the dispersion curves observed from the neutron and X-ray experiments is similar to that of a pure bilayer system (Fig. 2b). The same type of excitation curve has also been reported recently in bilayers with ethanol (Kaye et al. 2011). It can therefore be concluded that this type of dispersion relation is generic to lipid membranes, even in the presence of molecules, such as ethanol and cholesterol. Ethanol and cholesterol represent two different classes of molecules, i.e., ethanol molecules predominantly reside in the lipid-head group region, while cholesterol molecules interact extensively with the membrane's hydrophobic core. Although the dynamics of the lipid chains are altered by the presence of cholesterol, nevertheless, the membrane's basic characteristics seem to be preserved.

The lateral dynamics dispersion curve exhibits three characteristic regimes: a linear regime at small $q_{||}$, a minimum at a wavelength corresponding to the nearest-neighbor lipid tail distance, and finally, a second linear regime at large $q_{||}$. The linear regime at small $q_{||}$-values is related to a long wavelength sound-like propagation in the plane of the membrane. The corresponding excitations are thus longitudinal. The speed of sound is determined from the initial linear slope of the dispersion curve at small $q_{||}$-values up to the first maximum (see Fig. 2). Dynamics at small $q_{||}$ values are usually difficult to access in inelastic neutron scattering experiments because of the so-called kinematic restriction. It is related to the fact that energy and momentum of the neutrons are conserved during the scattering process and the parabolic shape of the energy as a function of $q_{||}$, $\hbar\omega = \hbar^2/(2m_n) \times q_{||}^2$, as for instance discussed in (Rheinstädter et al. 2004). While the absolute energies of the 5 mol% cholesterol dispersion relation in Fig. 6a fall into the accessible range, the energies significantly increase in the presence of 40 mol% cholesterol, such that the corresponding excitations were no longer accessible. The determination of the speed of sound is, therefore, beyond the scope of this study. Dynamics at higher $q_{||}$ values around the dispersion minimum and beyond are the domain of inelastic neutron scattering. The final linear regime of the dispersion relation corresponds to a propagating mode with predominantly transverse properties. In the case of pure lipid membranes, the slope or propagation velocity in this region is small. The maxima and minimum in the dispersion curve correspond to a crossover behavior, connecting these two propagating modes at small and large $q_{||}$. In particular, the flat region at the dispersion minimum may be related to a non-propagating standing-wave resulting from lipid tail dynamics with mixed longitudinal and transverse properties. The characteristics of these modes in pure lipid membranes have been previously reported (Kaye et al. 2011).

The introduction of cholesterol to the lipid membrane leads to additional propagating modes, as shown in Fig. 5. Because the inclusion of additional components increases the system's degrees of freedom, it is natural to expect that the addition of cholesterol will result in more dynamic modes, as shown in Fig. 6. One interesting observation is that the dispersion curves all exhibit the same features, i.e., two linear regimes at small and large $q_{||}$ connected by a crossover regime with two maxima and a minimum. This strongly suggests that these features are generic to such systems. We therefore speculate that they are related to the fact that lipid membranes are self-assembled layered structures whose properties are closely related to that of smectic liquid crystals.

It is interesting to note that the dispersion curve, shown in Fig. 6, resembles the energy of a quasiparticle in superfluid helium, where the parabolic minimum part of the spectrum is termed the roton [see, e.g., (Annet 2004)]. The different behavior of the dispersion curves indicates different modes of molecular motions. Comparing to superfluid helium, we can speculate that the linear phonon-like dispersion curve implies that the motion of the molecules are rigidly coupled, leading to a propagating sound-like wave. On the other hand, the parabolic dispersion curve near the minimum may indicate a different type of collective mode in which a moving molecule couples strongly

to its neighbors. As one molecule moves, the neighboring molecules must move out of its way, leading to a different collective mode of motion, as depicted in Fig. 7. Phenomenologically, the minimum of the dispersion curves is well described by a parabola [Eq. (5)]. The coefficient α of the parabola can thus be viewed as a parameter characterizing the generalized rigidity of the system on the nanometer-length scale. It is interesting to note that increasing the cholesterol content in the system leads to larger α in the gel and fluid branches of the dispersion curve, and a smaller α in the liquid-ordered branch. The energy offset ω_0 in the dispersion minimum, corresponding to the roton energy gap, can be related to the excitation energy of a "soft-mode." The occurrence of a soft mode often indicates a structural phase transition if the energy cost of this mode goes to zero, i.e., $\omega_0 = 0$. A smaller value of ω_0 might then be related to a structure with a higher degree of order; a full analysis of this feature will be presented in a future paper.

Some qualitative conclusions can be drawn from the data and the phenomenological analysis: From the values for α and ω_0 shown in Table 2, one can speculate that the gel phase has, not surprisingly, a higher degree of order and is considerably stiffer than the fluid phase. The addition of cholesterol has two distinct effects: it makes the chain dynamics in both phases stiffer (α increases by a factor of $\sim$2 between 5 and 40 mol% cholesterol), while at the same time, ω_0 also increases significantly, pointing to a more disordered molecular structure. The high cholesterol content liquid-ordered phase combines low values for α, corresponding to soft nanoscale dynamics, and at the same time, low values of ω_o, indicating a high level of order in the system. As has been previously speculated, the liquid-ordered phase seems to combine properties of rigid gel and soft fluid bilayers. In IXS experiments (Weiss et al. 2003; Chen et al. 2003), the addition of cholesterol leads to a significant increase in the high-frequency sound speed, pointing to a more rigid state at large length scales (small $q_{\|}$-values).

In Fig. 6 we observe the coexistence of excitations of gel, fluid and liquid-ordered phases. The separation of saturated and unsaturated phosphatidylcholine/cholesterol mixtures into nanometer-sized liquid-ordered and liquid-disordered phases was reported recently from MD simulations (de Meyer et al. 2010; Risselada 2008; Herrera 2012). Cholesterol was also found to collectively self-organize in phospholipid membranes (Martinez-Seara et al. 2010), which can also lead to a dynamic phase separation on the nanometer scale. These small (3–50 nm) and transient (nano- microsecond) heterogeneities in membranes are very difficult to resolve with standard experimental techniques. Inelastic neutron-scattering experiments on DMPC reported evidence for the co-existence of small nanometer gel and fluid domains in the temperature range of the main phase transition (Rheinstädter et al. 2004a)—based on the co-existence of the corresponding excitations in the spectra. Such domains were also found in MD simulations (Murtola et al. 2006; Ehrig et al. 2011). Recently, Armstrong et al. (2012) have used the coherence length of neutrons to observe co-existing gel and fluid domains in a phospholipid bilayer over a range of temperatures. The authors speculated that these small transient domains could be responsible for the so-called pseudo-critical behavior in phospholipid bilayers. The results in Fig. 6 now represent experimental evidence for the coexistence of gel, fluid and liquid-ordered phases in DMPC membranes containing different amounts of cholesterol. The corresponding domains can be speculated to be nanometer sized and short-lived.

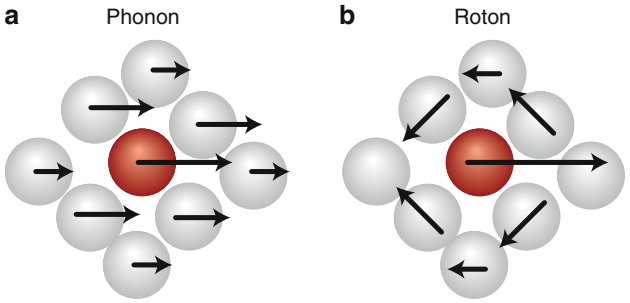

Fig. 7 **a** Molecular dynamics of particles participating in the propagating sound-like wave, i.e., the longitudinal phonon at small $q_{\|}$-values (*long length scales*) and **b** in the "roton" at $q_{\|}$-values in the dispersion minimum. These dynamics are expected to show a mixed, longitudinal and transverse character as neighboring particles couple strongly. Figure adapted from Annett (2004)

Conclusion

In summary, we present a neutron-scattering study of the lateral nanoscale dynamics in phospholipid membranes containing 5 and 40 mol% cholesterol. By measuring the excitation spectrum at several lateral $q_{\|}$ values (up to $q_{\|} = 3$ Å^{-1}), complete dispersion relations corresponding to gel, fluid and liquid-ordered bilayers were determined. The dispersion relations have a generic shape in single component lipid bilayers, i.e., there is an initial linear regime because of high-speed sound propagation and a second linear regime at high $q_{\|}$. The two linear regimes are connected by a maximum before a minimum is observed around nearest-neighbor distances between to lipid tails. The generic shape of these dispersion curves is preserved in the presence of cholesterol. A coexistence of excitations corresponding to gel, fluid and liquid-ordered phases was also observed. We therefore speculate the coexistence of

nanometer-sized, and possibly transient, gel, fluid and l_o domains in membranes containing cholesterol. Such nanodomains have long been previously suggested, with evidence coming from computer simulations and more recently from experiment (Simons 1997; Murtola et al. 2006; Ehrig et al. 2011; Armstrong et al. 2012; Engelma 2005; Eggeling et al. 2009; Lingwood 2010).

The region around the dispersion minimum was fitted using a phenomenological parabolic fitting method. The two parameters, i.e., the slope and the energy offset, were related to the bilayer's elastic properties on distances corresponding to hydrocarbon tail distances and molecular order. The inclusion of cholesterol has a distinct effect on the collective dynamics of the lipid hydrocarbon chains. Namely, we observe a pronounced stiffening of the membrane on nanometer length scales in both the gel and fluid phases, and also greater molecular disorder. For the first time, we have determined the nanoscale dynamics in the high-cholesterol liquid-ordered phase of DMPC bilayers. This phase seems to combine the properties of the gel and fluid phases, appearing softer than the fluid phase, but better ordered than the gel phase. Future experiments will offer a more complete description of these features, and a quantitative model will be put forth regarding the molecular properties of multi-component lipid bilayers.

Acknowledgments This research was funded by the Natural Sciences and Engineering Research Council of Canada (NSERC), the National Research Council Canada (NRC), the Canada Foundation for Innovation (CFI) and the Ontario Ministry of Economic Development and Innovation. John Katsaras is supported by Oak Ridge National Laboratory's (ORNL) Program Development (PD) and Laboratory Directed Research and Development (LDRD) programs.

References

Adachi T (2000) A new method for determining the phase in the X-ray diffraction structure analysis of phosphatidylcholine:alcohol. Chem Phys Lipids 107:93–97

Almeida P, Vaz W, Thompson T (1992) Lateral diffusion in the liquid phases of dimyristoylphosphatidylcholine/cholesterol lipid bilayers: a free volume analysis. Biochemistry 31:6739–6747

Annett JF (2004) Superconductivity, superfluids and condensates. Oxford University Press, Oxford

Armstrong CL, Sandqvist E, Rheinstadter MC (2011) Protein-protein interactions in membranes. Protein Pept Lett 18:344–353

Armstrong C, Barrett M, Toppozini L, Kucerka N, Yamani Z, Katsaras J, Fragneto G, Rheinstädter MC (2012) Co-existence of gel and fluid lipid domains in single-component phospholipid membranes. Soft Matter 8:4687–4694

Bayerl T (2000) Collective membrane motions. Curr Opin Colloid Interface Sci 5:232–236

Bloom M, Bayerl T (1995) Membranes studied using neutron scattering and NMR. Can J Phys 73:687–696

Brown DA, London E (2000) Structure and function of sphingolipid- and cholesterol-rich membrane rafts. J Biol Chem 275:17221–17224

Brüning B, Rheinstädter MC, Hiess A, Weinhausen B, Reusch T, Aeffner S, Salditt T (2010) Influence of cholesterol on the collective dynamics of the phospholipid acyl chains in model membranes. Eur Phys J E 31:419–428

Chen S, Liao C, Huang H, Weiss T, Bellisent-Funel M, Sette F (2001) Collective dynamics in fully hydrated phospholipid bilayers studied by inelastic X-ray scattering. Phys Rev Lett 86:740–743

Chen PJ, Liu Y, Weiss TM, Huang HW, Sinn H, Alp EE, Alatas A, Said A, Chen SH (2003) Studies of short-wavelength collective molecular motions in lipid bilayers using high resolution inelastic X-ray scattering. Biophys Chem 105:721–741

de Meyer F, Smit B (2009) Effect of cholesterol on the structure of a phospholipid bilayer. Proc Natl Acad Sci USA 106:3654–3658

de Meyer FJM, Benjamini A, Rodgers JM, Misteli Y, Smit B (2010) Molecular simulation of the dmpc-cholesterol phase diagram. J Phys Chem B 106:10451–10461

Eggeling C, Ringemann C, Medda R, Schwarzmann G, Sandhoff K, Polyakova S, Belov VN, Hein B, von Middendorf C, Schönle A, Hell SW (2009) Direc observation of the nanoscale dynamics of membrane lipids in a living cell. Nature 457:1159–1162

Ehrig J, Petrov EP, Schwille P (2011) Phase separation and near-critical fluctuations in two-component lipid membranes: Monte Carlo simulations on experimentally relevant scales. New J Phys 13:045019

Engelman DM (2005) Membranes are more mosaic than fluid. Nature 438:578–580

Fragneto G, Rheinstädter M (2007) Structural and dynamical studies from bio-mimetic systems: an overview. CR Phys 8:865–883

Harroun T, Katsaras J, Wassall S (2006) Cholesterol hydroxyl group is found to reside in the center of a polyunsaturated lipid membrane. Biochemistry 45:1227–1233

Harroun T, Katsaras J, Wassall S (2008) Cholesterol is found to reside in the center of a polyunsaturated lipid membrane. Biochemistry 47:7090–7096

Herrera FE, Pantano S (2012) Structure and dynamics of nano-sized raft-like domains on the plasma membrane. J Chem Phys 136:1–33

Hildenbrand MF, Bayerl TM (2005) Differences in the modulation of collective membrane motions by ergosterol, lanosterol, and cholesterol: a dynamic light scattering study. Biophys J 88:3360–3367

Hirn RB, Bayerl TM (1999) Collective membrane motions in the mesoscopic range and their modulation by the binding of a monomolecular protein layer of streptavidin studied by dynamic light scattering. Phys Rev E 59:5987–5994

Hirn R, Bayerl T, Rädler J, Sackmann E (1999) Collective membrane motions of high and low amplitude, studied by dynamic light scattering and micro-interferometry. Faraday Discuss 111:17–30

Huang J, Feigenson GW (1999) A microscopic interaction model of maximum solubility of cholesterol in lipid bilayers. Biophys J 76:2142–2157

Hub JS, Salditt T, Rheinstädter MC, de Groot BL (2007) Short range order and collective dynamics of DMPC bilayers. acomparison between molecular dynamics simulations, X-ray, and neutron scattering experiments. Biophysical J 93:3156–3168

Katsaras J (1998) Adsorbed to a rigid substrate, dimyristoylphosphatidylcholine multibilayers attain full hydration in all mesophases. Biophys J 75:2157–2162

Kaye MD, Schmalzl K, Nibali VC, Tarek M, Rheinstädter MC (2011) Ethanol enhances collective dynamics of lipid membranes. Phys Rev E 83:050,907

King GI, Worthington CR (1971) Analytic continuation as a method of phase determination. Phys Lett 35A:259–260

König S, Pfeiffer W, Bayerl T, Richter D, Sackmann E (1992) Molecular dynamics of lipid bilayers studied by incoherent quasi-elastic neutron scattering. J Phys II France 2:1589–1615

König S, Sackmann E, Richter D, Zorn R, Carlile C, Bayerl T (1994) Molecular dynamics of water in oriented dppc multilayers studied by quasielastic neutron scattering and deuterium-nuclear magnetic resonance relaxation. J Chem Phys 100:3307–3316

König S, Bayerl T, Coddens G, Richter D, Sackmann E (1995) Hydration dependence of chain dynamics and local diffusion in l-alpha-dipalmitoylphosphtidylcholine multilayers studied by incoherent quasi-elastic neutron scattering. Biophys J 68:1871–1880

Kučerka N, Marquardt D, Harroun T, Nieh MP, Wassall S, Katsaras J (2009) The functional significance of lipid diversity: orientation of cholesterol in bilayers is determined by lipid species. J Am Chem Soc 131:16358–16359

Kučerka N, Liu Y, Chu N, Petrache HI, Tristram-Nagle S, Nagle JF (2005) Structure of fully hydrated fluid phase DMPC and DLPC lipid bilayers using X-ray scattering from oriented multilamellar arrays and from unilamellar vesicles. Biophys J 88:2626–2637

Léonard A, Escrive C, Laguerre M, Pebay-Peyroula E, Néri W, Pott T, Katsaras J, Dufourc EJ (2001) Location of cholesterol in dmpc membranes. a comparative study by neutron diffraction and molecular mechanics simulation. Langmuir 17:2019–2030

Lindahl E, Edholm O (2000) Mesoscopic undulations and thickness fluctuations in lipid bilayers from molecular dynamics simulations. Biophys J 79:426–433

Lingwood D, Simons K (2010) Lipid rafts as a membrane-organizing principle. Science 327:46–50

Lipowsky, R, Sackmann, E (eds) (1995) Structure and dynamics of membranes, handbook of biological physics. vol 1, Elsevier, Amsterdam

Martinez-Seara H, Róg T, Karttunen M, Vattulainen I, Reigada R (2010) Cholesterol induces specific spatial and orientational order in cholesterol/phospholipid membranes. PLoS ONE 5:e11162

Meinhold L, Smith JC, Kitao A, Zewail AH (2007) Picosecond fluctuating protein energy landscape mapped by pressure-temperature molecular dynamics simulation. Proc Natl Acad Sci USA 104:17261–17265

Mihailescu M, Soubias O, Worcester D, White S, Gawrisch K (2011) Structure and dynamics of cholesterol-containing polyunsaturated lipid membranes studied by neutron diffraction and nmr. J Membr Biol 239:63–71

Mouritsen O (2010) The liquid-ordered state comes of age. Biochim Biophys Acta 1798:1286–1288

Murtola T, Róg T, Falck E, Karttunen M, Vattulainen I (2006) Transient ordered domains in single-component phospholipid bilayers. Phys Rev Lett 97:238102

Nagle JF, Wiener MC (1989) Relations for lipid bilayers. Biophys J 55(55):309–313

Nagle J, Zhang R, Tristram-Nagle S, Sun W, Petrache H, Suter R (1996) X-ray structure determination of fully hydrated lα phase dipalmitoylphosphatidylcholine bilayers. Biophys J 70:1419–1431

Nevzorov A, Brown M (1997) Bilayers from comparative analysis of 2H and 13C NMR relaxation data as a function of frequency and temperature. J Chem Phys 107:10288–10310

Pabst G, Kučerka N, Nieh MP, Rheinstädter M, Katsaras J (2010) Applications of neutron and X-ray scattering to the study of biologically relevant model membranes. Chem Phys Lipids 163(6):460–479

Paciaroni A, Orecchini A, Cornicchi E, Marconi M, Petrillo C, Haertlein M, Moulin M, Schober H, Tarek M, Sacchetti F (2008) Fingerprints of amorphous ice-like behavior in the vibrational density of states of protein hydration water. Phys Rev Lett 101:148104

Papanikolaou B, Papafotika A, Murphy C, Papamarcaki T, Tsolas O, Drab M, Kurzchalia TV, Kasper M, Christoforidis S (2005) Cholesterol-dependent lipid assemblies regulate the activity of the ecto-nucleotidase cd39. J Biol Chem 28:26406–26414

Paula S, Volkov A, Van Hoek A, Haines T, Deamer D (1996) Permeation of protons, potassium ions, and small polar molecules through phospholipid bilayers as a function of membrane thickness. Biophys J 70:339–348

Petrie R, Schnetkamp P, Patel K, Awasthi-Kalia M, Deans J (2000) Transient translocation of the b cell receptor and src homology 2 domain-containing inositol phosphatase to lipid rafts: evidence toward a role in calcium regulation. J Immunol 165:1220–1227

Pfeiffer W, Henkel T, Sackmann E, Knorr W (1989) Local dynamics of lipid bilayers studied by incoherent quasi-elastic neutron scattering. Europhys Lett 8:201–206

Pfeiffer W, König S, Legrand J, Bayerl T, Richter D, Sackmann E (1993) Neutron spin echo study of membrane undulations in lipid multibilayers. Europhys Lett 23:457–462

Pike L (2006) Rafts defined: a report on the keystone symposium on lipid rafts and cell function. J Lipid Res 47:1597–1598

Pike L (2009) The challenge of lipid rafts. J Lipid Res 50:S323–S328

Rheinstädter MC (2008) Collective molecular dynamics in proteins and membranes. Biointerfaces 3:FB83–FB90

Rheinstädter MC, Ollinger C, Fragneto G, Demmel F, Salditt T (2004a) Collective dynamics of lipid membranes studied by inelastic neutron scattering. Phys Rev Lett 93:108107

Rheinstädter MC, Ollinger C, Fragneto G, Salditt T (2004) Collective dynamics in phospholipid bilayers investigated by inelastic neutron scattering: exploring the dynamics of biological membranes with neutrons. Phys B 350:136–139

Rheinstädter MC, Seydel T, Demmel F, Salditt T (2005) Molecular motions in lipid bilayers studied by the neutron backscattering technique. Phys Rev E 71:061,908

Rheinstädter MC, Häussler W, Salditt T (2006a) Dispersion relation of lipid membrane shape fluctuations by neutron spin-echo spectrometry. Phys Rev Lett 97:048103

Rheinstädter MC, Seydel T, Häußler W, Salditt T (2006b) Exploring the collective dynamics of lipid membranes with inelastic neutron scattering. J Vac Sci Technol A 24:1191–1196

Rheinstädter MC, Seydel T, Salditt T (2007) Nanosecond molecular relaxations in lipid bilayers studied by high energy resolution neutron scattering and in-situ diffraction. Phys Rev E 75:011907

Rheinstädter MC, Schmalzl K, Wood K, Strauch D (2009) Protein-protein interaction in purple membrane. Phys Rev Lett 103:128104

Ridsdale A, Denis M, Gougeon PY, Ngsee JK, Presley JF, Zha X (2006) Cholesterol is required for efficient endoplasmic reticulum-to-golgi transport of secretory membrane proteins. Mol Biol Cell 17:1593–1605

Risselada HJ, Marrink SJ (2008) The molecular face of lipid rafts in model membranes. Proc Natl Acad Sci USA 105:17367–17372

Róg T, Pasenkiewicz-Gierula M, Vattulainen I, Karttunen M (2009) Ordering effects of cholesterol and its analogues. Biochim Biophys Acta 1788:97–121

Salditt T (2000) Structure and fluctuations of highly oriented phospholipid membranes. Curr Opin Colloid Interface Sci 5:19–26

Simons K, Ikonen E (1997) Functional rafts in cell membranes. Nature 387:569–572

Takeda T, Kawabata Y, Seto H, Komura S, Gosh S, Nagao M, Okuhara D (1999) Neutron spin echo investigations of membrane undulations in complex fluids involving amphilphiles. J Phys Chem Solids 60:1375–1377

Tarek M, Tobias D, Chen SH, Klein M (2001) Short wavelength collective dynamics in phospholipid bilayers: a molecular dynamics study. Phys Rev Lett 87:238101

Thewalt JL, Bloom M (1992) Phosphatidylcholine: cholesterol phase diagrams. Biophys J 63:1176–1181

Tristram-Nagle S, Liu Y, Legleiter J, Nagle JF (2002) Structure of gel phase dmpc determined by X-ray diffraction. Biophys J 83:3324–3335

Vist R, Davis JH (1990) Phase equilibria of cholesterol/dipalmitoylphosphatidylcholine mixtures: 2 h nuclear magnetic resonance and differential scanning calorimetry. Biochemistry 29:451–464

Weiss T, Chen PJ, Sinn H, Alp E, Chen S, Huang H (2003) Collective chain dynamics in lipid bilayers by inelastic X-ray scattering. Biophys J 84:3767–3776